The Effect of Quantization and Coulomb Friction on the Stability of Haptic Rendering

Nicola Diolaiti*, Günter Niemeyer†, Federico Barbagli‡, J. Kenneth Salisbury‡, Claudio Melchiorri*

*DEIS - University of Bologna, Italy, †Telerobotics Lab, Stanford University, USA, ‡AI-Robotics Lab, Stanford University, USA
ndiolaiti@deis.unibo.it, gunter.niemeyer@stanford.edu,
barbagli@robotics.stanford.edu, jks@robotics.stanford.edu, cmelchiorri@deis.unibo.it

Abstract

Rendering stiff virtual objects remains a core challenge in the field of haptics. A study of this problem is presented, which relates the maximum achievable object stiffness to the elements of the control loop. In particular, we examine how the sampling rate and quantization of position measurements interact with the inertia, natural viscous, and Coulomb damping of the haptic device. The resulting stability criterion generalizes previously known conditions. Simulations and experimental results support the theoretical analysis based on the passivity and describing function approaches.

1. Introduction

The field of haptics aims to provide the user with a sense of touch while interacting with simulated objects in a virtual world. It uses force feedback to render the mechanical features of the virtual objects, striving to reproduce the sensation of contact experienced with real objects.

Haptic devices are specifically designed to produce such forces and provide a transparent connection between the user and the artificial world. In particular, they exhibit low intrinsic friction and inertia to minimize dynamic distortion of the user's perception [1]. This generally necessitates low motor reduction ratios and efficient transmission elements. Performance may also be optimized trading off the number of actuated and sensed degrees of freedom (DOF) based on the expected application [2].

Connecting the user and haptic device to the virtual environment requires a feedback control system commonly implemented as a digital control loop. A typical system is depicted in Fig. 1 for a single degree of freedom. The computer interface entails time discretization and quantization of position and force information, inserts computational delays, and involves current amplification with limited bandwidth.

Rendering contact with a stiff virtual wall remains a key component and core challenge of haptics. This implies high gain feedback in the haptic control loop, which is particularly demanding for low inertia and friction devices. The afore-mentioned non-idealities limit performance and can lead to oscillatory or unstable behavior that destroys the illusion of virtual reality and may even be harmful to the operator.

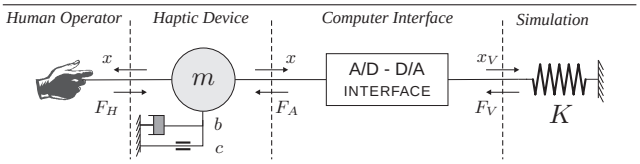

Figure 1. A single degree of freedom haptic interface rendering a virtual stiffness

Passivity theory has been used in [3–5] to view some of these limitations and provide stability conditions; passivity is sufficient for stability if the operator is described by unknown passive elements [6]. The time delay introduced by the zero-order-hold generates and injects energy into the system. This excess energy may cause instability if not dissipated by the haptic device's intrinsic friction or through control [7]. These concepts are refined in [8] to consider computational delay, in [9] to include Coulomb friction and variable stiffness, while quantization effects are accounted in [10].

This work aims to relate the achievable performance, measured as the largest stable feedback, to the parameters characterizing the main non-idealities of the control loop. It accounts for the non-linearities introduced by the position quantization and the dynamic Coulomb friction in the mechanism. The passivity analysis introduced in [11] is here integrated with an approximate analysis based on describing function techniques, to show that, depending on other parameters such as the sampling frequency and the intrinsic viscous friction, the rendering of a stiff virtual object can be passive, locally stable, oscillating or unstable. Computational delays and limited amplifier's bandwidth, even if not directly considered in this paper, could be easily accounted especially by means of the describing function approach. Simulation and experimental data are shown to support the theoretical findings. We hope this will facilitate both device designers and programmers alike to create effective haptic systems.

The paper is organized as follows: in Sect. 2 the problem is stated in detail and all elements and non-idealities are de-

fined. Sect. 3 presents the main results of the work, introducing the stability criterion for the haptic system, discussing its implications and its applications to common haptic devices. Simulations, Sect. 4, and experimental evidences obtained using a single degree of freedom device, validate the theoretical findings. The analytical proof of the required passivity and energy generation arguments is presented in Sect. 6, followed by the describing function analysis in Sect. 7. Final remarks and future work are discussed in Sect. 8.

2. Problem Statement

2.1. System Description

It is a common goal in the field of haptics to render contact with a seemingly rigid virtual wall. This is generally accomplished by simulating a stiff spring force that is displayed to the user through the haptic device while the virtual contact is sustained. Our developments study the maximum achievable wall stiffness and its relation to the computer interface and device parameters. As such, we focus on a single degree of freedom depicted in Fig. 1. The haptic device consists of a physical inertia m and has intrinsic friction, attributed to both viscous components b and dynamic Coulomb components c. Its position x and velocity $\dot{x}$ result from the force F_H applied by the human operator and the force F_A exerted by the controller to simulate the virtual stiffness K.

A computer interface relates the continuous real device to the discrete virtual world. As many researchers have recognized, the elements constituting this interface can introduce oscillatory or unstable behaviors. Shown in Fig. 2, we examine quantization of the signal, discrete sampling at time intervals T and associated zero order hold, possible delays in computation of the virtual environment, and amplifier dynamics. While quantization may stem from both the input sensor and output D/A converter, we refer, without loss of generality, only to the encoder. The equivalent resolution of the D/A converter is generally substantially higher.

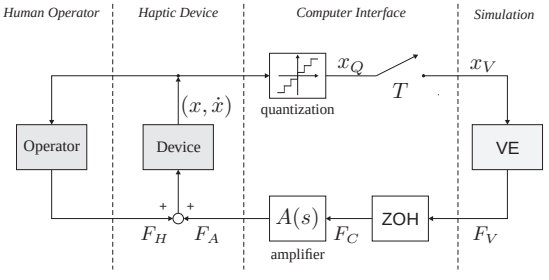

Figure 2. Block diagram of the haptic system, connecting the human user with the virtual spring

Signal		*Dimensionless Value*
Time	t	$\tau := \frac{t}{T}$
Position	x	$\xi := \frac{x}{\Delta}$
Velocity	$\dot{x}$	$\dot{\xi}(\tau) = \frac{d\xi(\tau)}{d\tau} = \frac{\dot{x}T}{\Delta}$
Force	F	$\varphi := \frac{F}{K\Delta}$

Parameter		*Dimensionless Value*
Mass	m	$\mu := \frac{m}{KT^2}$
Friction		
Viscous	b	$\beta := \frac{b}{KT}$
Coulomb	c	$\sigma := \frac{c}{K\Delta}$

Table 1. Dimensionless signals and parameters

The haptic device is modeled as a point mass and can be described by the differential equation

$$m\ddot{x}(t) + b\dot{x}(t) + c\,\mathrm{sgn}\left(\dot{x}(t)\right) = F_H(t) + F_A(t) \qquad (1)$$

Meanwhile, assuming no computational delay because of the simplicity of the control law, the virtual spring force is governed by:

$$F_V(h) = -K\Delta\left(\left\lfloor \frac{x(hT)}{\Delta} \right\rfloor + \frac{1}{2}\right) \qquad \forall h \in \mathbb{N} \qquad (2)$$

where T is the sampling time, h denotes the discrete time variable, Δ is the encoder resolution, and $\lfloor . \rfloor$ refers to the integer part. Note the spring is assumed to be bidirectional, which represents the worst case compared to a unidirectional wall. Alternatively, this may be interpreted relative to a steady state device position inside the virtual wall due to a constant bias force holding the device in contact. We place the origin $x = 0$ at the encoder boundary nearest the steady state position. Furthermore, we assume a residual bias of $1/2K\Delta$ in (2), so that the spring force is symmetric about the origin but finds no steady state value as $|F_V(h)| \geq \frac{1}{2}K\Delta$. This poses the most challenging boundary conditions for the controller. The zero order hold maintains this desired controller force during each servo cycle:

$$F_C(t) = F_V(h) \qquad \forall t \in [hT; (h+1)T[\,,\ h \in \mathbb{N} \qquad (3)$$

Finally, according to what discussed in the introduction, we assume no limitations in the amplifier's bandwidth, hence $F_A(t) = F_C(t)$.

2.2. Dimensionless Parametrization

To reduce the number of parameters, we perform a dimensional analysis. In particular, we measure position relative to a single encoder quantum Δ, time relative to the sampling interval T, and force relative to the smallest force step $K\Delta$ matching one encoder tick. Velocity is expressed relative to one encoder quantum per sampling interval Δ/T. The resulting dimensionless signals as well as device and interface parameters are summarized in Table 1.

Accordingly, the differential equation (1) may be rewritten as:

$$\mu\ddot{\xi}(\tau) + \beta\dot{\xi}(\tau) + \sigma\,\mathrm{sgn}\left(\dot{\xi}(\tau)\right) = \varphi_H(\tau) + \varphi_A(\tau) \qquad (4)$$

while the applied controller force simplifies to:

$$\varphi_A(\tau) = -\lfloor \xi(h) \rfloor - \frac{1}{2} \qquad \forall \tau \in [h;\ h+1[\tag{5}$$

2.3. Stability Approach

Haptic systems are typically analyzed in the framework of passivity, which provides a powerful tool showing that combinations of passive elements are also passive and feedback loops of two passive elements are stable. We follow this tradition while noting that a human operator is not passive and hence the stability of the haptic interaction can not be immediately assumed. Fortunately common experience shows that humans are skilled at interacting with passive objects and do so in a stable fashion [6].

More specifically, a human operator will actively move at frequencies below 10 Hz and may generate energy. But in this low frequency band the inertia and friction of the mechanism together with the simple virtual spring appear passive and interactions are stable. Effects of computer interface approximations and lag are negligible.

In contrast, at higher frequencies the artificial lag can cause substantial problems. Instabilities usually occur at several hundred Hertz. Here the user simply imposes an impedance on the system, consisting of stiffness, damping, and possibly added mass [12]. And while the impedance can change with the user's grip, it is not arbitrary; it necessarily contains relatively low stiffness and high damping. Hence, passivity of the system is not strictly necessary for stability, though it remains sufficient.

The damping added by the operator could be lumped together with the friction inherent to the device. As such, we consider the worst case scenario with minimal damping, in which the user is not or barely touching the haptic device; the user adds negligible impedance to the system. This matches practical experiences, where a heavy grip stabilizes a system while a light grip is the most challenging. Therefore, we focus on the passivity and stability of the internal haptic loop connecting the virtual spring to the device inertia.

3. Main Results

The main stability criterion, derived from the passivity and the describing function analysis and supported by simulation and experimental work, is stated and its implications discussed. In particular, the stability criterion will be used to interpret, on the basis of their physical parameters, the performances that can be achieved by common haptic devices.

The haptic control system depicted in Fig. 2 with zero delay is stable if:

$$\left(\beta - \frac{1}{2}\right) + \left|\dot{\xi}_0\right|^{-1} \left(\sigma - \frac{1}{2}\right) \geq 0 \quad \text{and} \quad \sigma \geq \frac{1}{2} \tag{6}$$

where $|\dot{\xi}_0|$ represents the maximum system velocity. For a stable system, we can without loss of generality assume this occurs at time τ=0. For a stable limit cycle, this velocity will be repeated at later times but is never exceeded. As the maximum velocity occurs at zero acceleration and hence zero force, we can further assume a zero initial position (ξ_0=0). These initial conditions may also be interpreted as the moment of impact when deceleration begins.

If the haptic control system is sampled without quantization, the stability criterion relaxes to

$$\left(\beta - \frac{1}{2}\right) + \left|\dot{\xi}_0\right|^{-1} \sigma \geq 0 \tag{7}$$

3.1. Interpretation

The inequalities (7) and (6) can be seen as generalizing Colgate's inequality (β>1/2 in the dimensionless formulation) [4] to include dynamic Coulomb friction and sensor quantization. From (7) we see in particular that Coulomb friction may assist viscous damping especially for small velocities, consistent with physical intuition. We also see qualitative distinctions between the two dissipation effects. From (6), the viscous friction:

$$\beta \geq \frac{1}{2} \qquad \Rightarrow \qquad b \geq \frac{KT}{2} \tag{8}$$

should balance the stiffness and effective delay due to the sampling and zero order hold; the phase lag of the zero order hold is compensated by the phase lead of the viscosity. Coulomb friction:

$$\sigma \geq \frac{1}{2} \qquad \Rightarrow \qquad c \geq \frac{K\Delta}{2} \tag{9}$$

must dominate the step force changes due to quantization to avoid limit cycles.

The general combination of the two dissipations is best viewed on the (β, σ) plane. Different regions demonstrate different behavior, as depicted in Fig. 3.

We first note from derivations in Sect. 6 that at every instant of time τ power can not be generated if

$$\sigma - \frac{1}{2} \geq -\left|\dot{\xi}(\tau)\right| \left(\beta - \frac{1}{2}\right) \tag{10}$$

This critical line intersects the point ($\beta = 1/2$, $\sigma = 1/2$) with a slope of $-|\dot{\xi}(\tau)|$. It rotates between vertical (when $\dot{\xi} \to \infty$) and horizontal (when $\dot{\xi} \to 0$). The individual regions describe the behavior of the system, if it is operating at the (β, σ) values.

(a) β>1/2, σ>1/2: In this region the haptic loop is globally stable. It is the only region in which the resulting system is passive (no energy generation regardless of velocity and initial conditions). Indeed it is characterized by high values of both viscous and Coulomb friction that satisfy both (8) and (9).

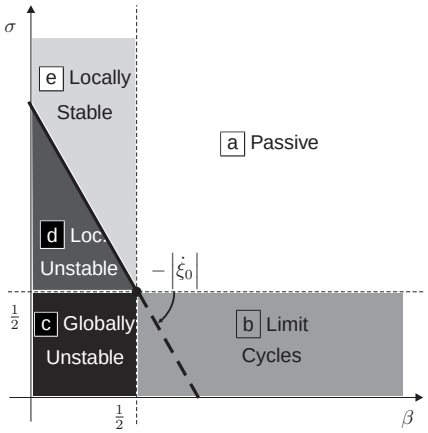

Figure 3. Stability regions of the (β, σ) plane.

(b) $\beta{>}1/2$, $\sigma{<}1/2$: This region gives rise to stable self-sustained oscillations (limit cycles). At any operating point, decaying velocities $\dot{\xi}(\tau)$ rotate the critical line (10) counter clockwise until power generation occurs and supports the motion. The resulting energy production renders the operating point non-passive, though the system remains stable. The magnitude of the limit cycle is furthermore limited below a single encoder tick, so that the user may not observe the vibration or may dampen it out.

(c) $\beta{<}1/2$, $\sigma{<}1/2$: With both viscous and Coulomb friction below their respective limits, systems operating in this region may generate energy at all times. The describing function analysis confirms that the system is unstable and at least under a light touch the haptic user interaction will also be unstable.

(d) $\beta{<}1/2$, $1/2{<}\sigma{<}1/2{+}|\dot{\xi}_0|(1/2{-}\beta)$: Operating points below the critical line (10) again generate power. However, unlike region (b), operating points that start below the line will always remain below the line and are unstable. The instability is marked as local as it only occurs if the initial velocity places the critical line above the operating point.

(e) $\beta{<}1/2$, $\sigma{>}1/2{+}|\dot{\xi}_0|(1/2{-}\beta)$: In the final region, operating points are locally stable. Starting with a velocity that places the critical line (10) below the operating point prevents energy generation at all times and leads to a stable loop. Like region (b) this area is not passive, as its behavior depends on the initial velocity, but it creates a stable haptic loop and a stable interaction with the user.

The condition (6) may also be viewed in the dimensioned form:

$$\left(b-\frac{KT}{2}\right)+|\dot{x}_0|^{-1}\left(c-\frac{K\Delta}{2}\right)\geq 0 \text{ and } c\geq\frac{K\Delta}{2} \quad (11)$$

and the impact of the parameters K, Δ, and T on the system behavior can be evaluated. Both β and σ depend equally on K, so that a stiffness increase moves an the operating point in a straight line toward the origin, thus decreasing its distance from the unstable region. Meanwhile an increase of the sampling frequency moves the point to the right horizontally and a reduction of Δ corresponds to a vertical movement thus improving the stability of the overall system.

3.2. Application to common devices

We find that most haptic devices in practice operate in region (e). Identification procedures analogous to those presented in [13], allowed to estimate friction coefficients of different commercially available devices and to relate them to the maximum stiffness that can be rendered without oscillations and without human grasping. The devices taken into account are the Omega and the Delta from Force Dimension, the Impulse Engine 2000 force-feedback joystick from Immersion, the Toolhandle [14] device and the Phantom 1.0 [1] from Sensable. Collected data are summarized in Table 2, where the corresponding dimensionless parameters are also shown. Note that in all cases, except the Impulse Engine, the estimated viscous friction coefficients were essentially bounded by the resolution of the measurement instruments and of the estimation techniques.

Device	m *[Kg]*	b *[Ns/m]*	c *[N]*	Δ *[μm]*	T *[ms]*	K *[N/m]*	μ	β	σ
Omega	0.220	0.01	0.147	10	0.33	14500	136.6	0.002	1.01
Delta	0.250	0.01	0.883	30	0.33	14500	155.2	0.002	2.03
Impulse Engine	0.032	0.02	0.024	31.4	0.2	800	1007.8	0.13	0.97
Phantom 1.0	0.072	0.005	0.038	29.1	1	1015	70.55	0.004	1.29
Toolhandle	0.119	0.001	0.034	20.1	1	3125	38.19	0.0003	0.54
Human Operator	0.150	4.8				600			

Table 2. Dimensionless parameters of common devices

At high stiffnesses, common servo-rates and without human grip, the dissipation is dominated entirely by Coulomb friction, which works well at low speeds. However, should the system ever experience a large initial velocity:

$$\dot{\xi}_0 > \frac{\sigma-1/2}{1/2-\beta} \quad \Rightarrow \quad \dot{x}_0 > \frac{2c-K\Delta}{KT-2b} \quad (12)$$

it would become unstable and hence can not be described as passive. Since we are operating at the edge of stability, the actual velocities $\dot{\xi}_0$ were fairly low. On the other hand, higher velocities can be experienced only when the operator is moving the device. The last row of Table 2, taken from [12], shows the corresponding data of the human operator, that in the case of grasping sum to devices intrinsic parameters. Consistently with the discussion of Sect. 2.3 in this case the viscous friction, provided by the operator is substantial, thus helping the system to dissipate energy excess.

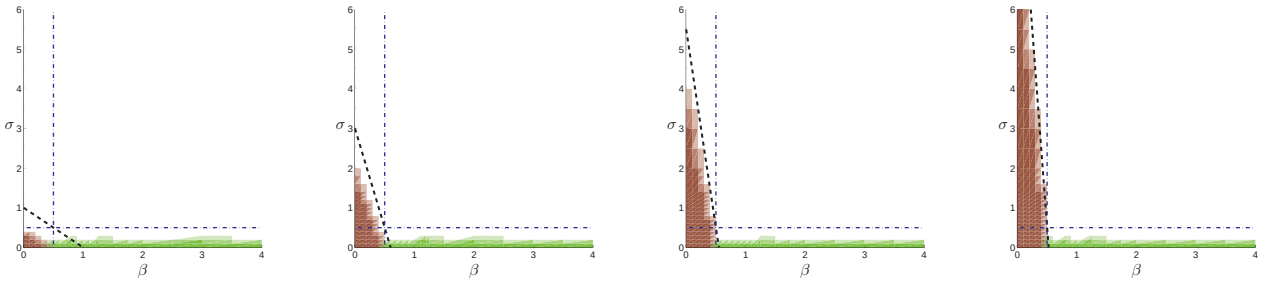

4.1: $\dot{\xi}_0 = 1$ 4.2: $\dot{\xi}_0 = 5$ 4.3: $\dot{\xi}_0 = 10$ 4.4: $\dot{\xi}_0 = 20$

Figure 4. Stability regions on the (β, σ) plane for $\mu = 100$: dark areas are points detected to be unstable, light areas are persisting oscillations, white areas are stable points for different values of $\dot{\xi}_0$.

4. Simulations

Before providing an analytical proof of the stability criterion (6), it is worth examining the simulation results. According to previous considerations, the dimensionless model (4) has been simulated assuming no initial deflection $\xi(0) = 0$, different initial velocities $\dot{\xi}(0)$, and a null input from the human operator. The stability of 714 couples of β and σ has been evaluated over the time interval $\tau = [0, 5 \times 10^4]$ corresponding to 50 sec. with a sampling time $T = 1$ ms.

Fig. 4 shows the results obtained with $\mu = 100$ and four different initial velocities. The dark areas represent, for each initial velocity, the regions of unstable behavior. The light areas represent regions of persisting oscillation. The white areas are regions of stable behavior. The irregular profile is due to the discrete number of points that have been simulated. The critical lines associated to each case are dashed, while the dash-dot lines are used to identify the regions of Fig. 3. A good correspondence between the predictions and the simulation outcomes can be noticed, also by recalling that (6) is the result of a worst case analysis and the system can be stable also in the region where (6) is not satisfied.

5. Experimental Results

Experimental validation of the proposed criterion has been carried out by means of a Maxon RE35 motor equipped with an encoder having 8192 counts per revolution. Since it is a rotative device, positions and forces in (1) correspond to angles and torques. The current amplifier, a Copley model 403, was commanded via a 14 bit D/A interface from the RTAI-Linux control loop. The amplifier was configured to have a bandwidth of 3 KHz, substantially larger than the servo rate that was changed to test different values of β up to 1 KHz. Different values of σ were obtained by artificially reducing the encoder resolution in the control software.

The estimation of friction parameters of the device leads to $b = 9 \times 10^{-6}$ Nm/rad sec, $c = 2 \times 10^{-3}$ Nm and $m = 6.28 \times 10^{-6}$ Kg m^2; since in this case the Coulomb dynamic friction is much larger than the viscous friction, analogously to other haptic interfaces presented in Table 2, the device is likely to operate in the locally stable/unstable regions (d)-(e) illustrated in Fig. 3.

Because of the simplicity of the virtual environment and the setup configuration, the computational delay and the limitations on amplifier's bandwidth were negligible, according to the assumptions underlying the criterion (6). The initial velocity determining the critical line on the (β, σ) plane is difficult to measure and reproduce. Accurate results have been obtained by setting an initial displacement for the virtual spring, which is bidirectional for these experiments. In particular, the spring preload is computed in such a way the initial energy of the system corresponds to the kinetic energy it would have with $\xi_0 = 0$ and the desired value of $\dot{\xi}_0$.

Fig. 5.1 through 5.3 show the outcomes obtained with points in different regions of the (β, σ) plane. The left portion of each figure shows the characteristic point and the critical line associated with the initial condition, while the right side shows the temporal diagram of the angular displacement. In this same diagram, the dashed horizontal lines correspond to ± 1 encoder tick. Starting from Fig. 5.1, we evaluated a point located in the globally stable region and, despite the high initial condition represented by the slope of the critical line, the position converges to the origin. Then, by simulating a very poor encoder resolution, the behavior of a point located in the limit cycle region is investigated, (Fig. 5.2) and as predicted, we observe a persistent oscillation bounded by the encoder resolution. By changing the initial conditions, the behavior of a point located in the locally stable region was finally studied in Fig. 5.4 and 5.3. As expected, the reduction of the initial energy stored into the digital spring, or alternatively of the impact velocity $\dot{\xi}_0$, stabilizes the haptic device.

6. Passivity Analysis of Digital Springs

Human beings are particularly used to dealing with passive objects in their every day life, and therefore the simu-

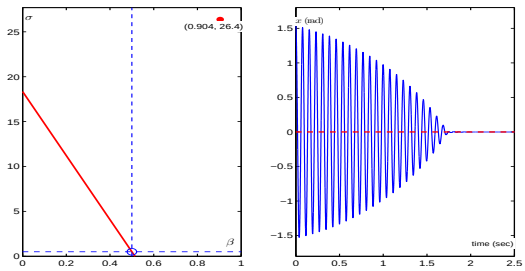

5.1: Region A: Passive behavior

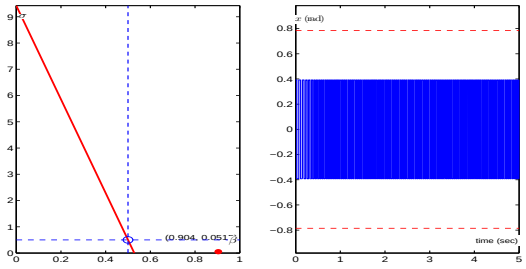

5.2: Region B: Persisting oscillation

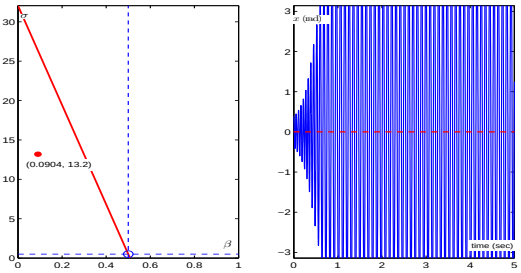

5.3: Region D: Locally unstable behavior

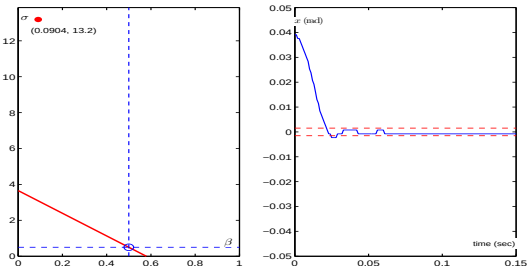

5.4: Region E: Locally stable behavior

Figure 5. Experimental results for the one DOF device: (β, σ) plane and corresponding trajectories

lation of passive objects (e.g. virtual walls) should be implemented in such a way that unrealistic oscillations that could destroy the illusion of interacting with real objects are avoided. Besides these considerations, if both the operator and the haptic display are passive systems, their feedback interconnection through the signals $\dot{x}(t)$ and $F_H(t)$ of Fig. 2 is still a passive, and therefore globally stable, system [15].

From an informal point of view, the system comprising the device, the computer interface and the virtual environment (see Fig. 2), is passive if only a finite amount of energy can be extracted by the user. However, previous work [3–5] showed that energy generation for a discrete time, non quantized virtual spring occurs because of the time delays introduced by the discrete time implementation of the virtual environment (Fig. 2). This fact violates the passivity condition.

From a formal point of view, by using the notion of dissipativity introduced by [16] and [15], the passivity of system (4) can be expressed by means of the inequality:

$$\int_{\tau_0}^{\tau_1} \varphi_H(\tau)\dot{\xi}(\tau)d\tau \geq \mathcal{H}_T(\tau_1) - \mathcal{H}_T(\tau_0) \qquad \forall \tau_1 \geq \tau_0 \tag{13}$$

where $\mathcal{H}_T(\tau) = \mathcal{H}_T(\xi(\tau), \dot{\xi}(\tau))$ is a positive definite function representing the energy stored in the system and $\varphi_H(\tau)\dot{\xi}(\tau)$ is the dimensionless instantaneous power exchanged with the human operator.

If we explicitly take into account the power $P_d(\tau)$ that is dissipated because of physical friction and the spurious power generation $P_g(\tau)$ due to the non-idealities in the control loop and in the computer interface, we have:

$$\begin{aligned}\int_{\tau_0}^{\tau_1} \varphi_H(\tau)\dot{\xi}(\tau)d\tau = \mathcal{H}_T(\tau_1) - \mathcal{H}_T(\tau_0) + \\ + \int_{\tau_0}^{\tau_1} P_d(\tau)d\tau - \int_{\tau_0}^{\tau_1} P_g(\tau)d\tau\end{aligned} \tag{14}$$

By comparing (13) with (14), the haptic display is passive iff the storage function $\mathcal{H}_T$ exists and the following dissipation inequality is satisfied:

$$\int_{\tau_0}^{\tau_1} P_d(\tau)d\tau \geq \int_{\tau_0}^{\tau_1} P_g(\tau)d\tau \qquad \forall \tau_1 \geq \tau_0 \tag{15}$$

6.1. Storage function of a quantized spring

As consequence of the previous discussion, a time continuous quantized spring is a lossless system, for which (13) holds as equality. According to the model (4), the total energy $\mathcal{H}_T(\xi, \dot{\xi})$ of the haptic display is given by the sum of the kinetic energy of the device and of the pseudo-elastic potential energy $\mathcal{H}_e(\xi)$ stored in the quantized spring:

$$\varphi_Q(\tau) = -\lfloor \xi(\tau) \rfloor - \frac{1}{2} \tag{16}$$

For the purposes of the following sections a bilateral spring will be assumed (i.e. the unilateral constraint is ignored). As noted in [4], the sufficiency of (15) holds also when the unilateral constraint representing the virtual wall is considered. The device is passive when the applied force φ_A is null and, when it is moving the dissipation provided

by intrinsic friction is larger than energy generation. Therefore φ_A can be set to zero at any time without affecting the energy balance.

To compute $\mathcal{H}_e(\xi)$, we rewrite the relation between the real and the quantized position as:

$$\xi = \lfloor \xi \rfloor + \rho \qquad 0 \leq \rho < 1 \tag{17}$$

where $\rho = \rho(\xi)$ represents the quantization error and is a function exclusively of the position ξ. Note that the static compensation of this error introduced in (5) and (16) has the effect to translate vertically the diagram so that the magnitude of the compensated error is bounded by 1/2, but does not alter the fact that ρ is a positional function. For this reason, $\mathcal{H}_e(\xi)$ is expressed by:

$$\mathcal{H}_e(\xi) = -\int \varphi_Q(\xi) d\xi = \frac{1}{2}\xi^2 + \frac{1}{2}\left(\rho(\xi) - \rho^2(\xi)\right) \tag{18}$$

where the term depending on $\rho(\xi)$ is always positive because $\rho \in [0;1[$. Finally $\mathcal{H}_T(\xi, \dot{\xi})$ is given by:

$$\mathcal{H}_T(\xi, \dot{\xi}) = \frac{1}{2}\mu\dot{\xi}^2 + \frac{1}{2}\left(\xi^2 + \rho(\xi) - \rho^2(\xi)\right) \tag{19}$$

6.2. Energy Leaks

The amount of energy $E_g(\tau_0, \tau_1)$ that is generated during the time interval $\tau \in [\tau_0; \tau_1[$ can be computed by comparing the energy variation of the digital spring (5) to its lossless time continuous counterpart φ_Q:

$$E_g(\tau_0,\tau_1) = \int_{\tau_0}^{\tau_1} P_g(\tau) d\tau = \int_{\tau_0}^{\tau_1} \left[\varphi_A(\tau) - \varphi_Q(\tau)\right] \dot{\xi}(\tau) d\tau \tag{20}$$

First of all we notice that, because of the zero-order-hold, the force (5) applied by the control algorithm to the device is constant for a sampling interval. Since the passivity inequality (15) has to be satisfied for every $\tau_1 \geq \tau_0$, the most convenient way to evaluate the time integral (20) is to set τ_0 to h and to assume $\tau_1 \in [h;\ h+1[$. The results obtained then have to hold for every $h \in \mathbb{N}$. In this way, $\varphi_A(\tau)$ is constant during the integration interval and (20) can be rewritten as:

$$E_g(h, \tau_1) = \int_h^{\tau_1} \left(\lfloor \xi(\tau) \rfloor - \lfloor \xi(h) \rfloor\right) \dot{\xi}(\tau) d\tau \tag{21}$$

By means of (17), we can split the contribution to energy generation E_{gz} due to discretization and the contribution E_{gq} given by quantization:

$$E_{gz} := \int_h^{\tau_1} \left(\xi(\tau) - \xi(h)\right) \dot{\xi}(\tau) d\tau \tag{22}$$

$$E_{gq} := \int_h^{\tau_1} \left(\rho(\tau) - \rho(h)\right) \dot{\xi}(\tau) d\tau \tag{23}$$

where $\rho(\tau) = \rho(\xi(\tau))$ for notational simplicity.

Straightforward computations show that, when the device is moving (i.e. $\xi(\tau_1) \neq \xi(h)$), the zero order hold always contributes to energy generation:

$$E_{gz} = \frac{1}{2}\Big(\xi(\tau_1) - \xi(h)\Big)^2 \tag{24}$$

Focusing now on E_{gq}, we recall that the quantization error $\rho(\xi(\tau))$ is a purely positional function and the following expression is obtained:

$$E_{gq} = \Big(\rho(h) - \frac{1}{2}\Big)\Big(\lfloor \xi(\tau_1) \rfloor - \lfloor \xi(h) \rfloor\Big) + \\ - \frac{1}{2}\Big(\rho(\tau_1) - \rho(h)\Big)^2 \tag{25}$$

Since in general $\rho(\tau)$ and $\lfloor \xi(\tau) \rfloor$ are independent quantities, it is possible now to compute the maximum of E_{gq} with respect to $\rho(h)$ and $\rho(\tau_1)$. Remembering that $\rho \in [0;1[$, from (25) we have:

$$E_{gq} \leq \frac{1}{2}\Big|\lfloor \xi(\tau_1) \rfloor - \lfloor \xi(h) \rfloor\Big|_{MAX} = \frac{1}{2}\Big|\xi(\tau_1) - \xi(h)\Big| \tag{26}$$

because the maximum is reached, depending whether the measured displacement $\lfloor \xi(\tau_1) \rfloor - \lfloor \xi(h) \rfloor$ is positive or negative, when $\rho(h) = \rho(\tau_1) = 0$ or $\rho(h) = \rho(\tau_1) = 1$.

Finally, by recalling (24), we can state that the generated energy is upperly bounded by:

$$E_g(h, \tau_1) \leq \frac{1}{2}\Big(\xi(\tau_1) - \xi(h)\Big)^2 + \frac{1}{2}\Big|\xi(\tau_1) - \xi(h)\Big| \tag{27}$$

6.3. Energy Dissipation

In the model (1) of the haptic interface, we took into account two main dissipative phenomena: viscous friction, modeled by the dimensionless parameter β, and the dynamic Coulomb friction σ. This modeling choice corresponds to a worst case scenario with respect to friction. Indeed, especially at low velocities, other phenomena like static Coulomb friction, Stribeck friction generally add other dissipation, thus helping the system to preserve its passivity, even if the overall transparency is affected. On the other hand, at low velocities the dynamic Coulomb friction is more efficient than the viscous friction in dissipating the energy excess generated by the digital spring and it has to be considered in order to obtain a more accurate estimate of the maximum achievable stiffness.

The amount of energy dissipated $E_d(h, \tau_1)$ by (4) during the same time interval considered in Sect. 6.2 is expressed by:

$$E_d(h,\tau_1) = \int_h^{\tau_1} P_d(\tau) d\tau = \int_h^{\tau_1} \Big[\beta\dot{\xi}^2(\tau) + \sigma|\dot{\xi}(\tau)|\Big]\, d\tau \tag{28}$$

A lower bound for the first term, representing dissipation due to viscous friction, can be obtained from the Cauchy-Schwarz inequality, that leads to:

$$\int_h^{\tau_1} \beta \dot{\xi}^2(\tau) d\tau \geq \beta \frac{\Big(\xi(\tau_1) - \xi(h)\Big)^2}{\tau_1 - h} \tag{29}$$

while the term due to the dynamic Coulomb friction is bounded by:

$$\int_h^{\tau_1} \sigma \left|\dot{\xi}(\tau)\right| d\tau \geq \sigma \left|\xi(\tau_1) - \xi(h)\right| \tag{30}$$

Therefore the lower bound on (28) is obtained by summing (29) and (30):

$$E_d \geq \beta \frac{\Big(\xi(\tau_1) - \xi(h)\Big)^2}{\tau_1 - h} + \sigma \left|\xi(\tau_1) - \xi(h)\right| \tag{31}$$

Note that (31) expresses that the friction effects along the path from $\xi(h)$ to $\xi(\tau_1)$ are minimized if the velocity is kept constant.

Finally, because $\tau_1 \in [h;\ h+1[$, a more conservative bound is expressed by:

$$E_d \geq \beta \Big(\xi(\tau_1) - \xi(h)\Big)^2 + \sigma \left|\xi(\tau_1) - \xi(h)\right| \tag{32}$$

6.4. Passivity Condition

The passivity condition (15) therefore reduces to the following worst-case inequality between the dissipated (32) and generated energy (27) during the considered time interval:

$$\Big(\beta - \frac{1}{2}\Big)\Big(\xi(\tau_1) - \xi(h)\Big)^2 + \Big(\sigma - \frac{1}{2}\Big)\left|\xi(\tau_1) - \xi(h)\right| \geq 0 \tag{33}$$

that has to be satisfied for every $\tau_1 \in [h;\ h+1[$ and for every h.

Note that when $\xi(\tau_1) = \xi(h)$ there is no energy generation, so we can divide both the left and the right hand of (33) by $|\xi(\tau_1) - \xi(h)|$. Moreover, since the velocity is a continuous function, the mean value theorem holds for $\tau \in [h; \tau_1[$:

$$\left|\xi(\tau_1) - \xi(h)\right| = (\tau_1 - h)\left|\dot{\xi}(\tau)\right| \leq \left|\dot{\xi}(\tau)\right| \tag{34}$$

and the dissipation inequality simplifies to:

$$|\dot{\xi}(\tau)|\Big(\beta - \frac{1}{2}\Big) + \Big(\sigma - \frac{1}{2}\Big) \geq 0 \tag{35}$$

that corresponds to (10), representing a line on the (β, σ) plane rotating, as the instantaneous velocity $\dot{\xi}(\tau)$ changes, about the point $(1/2, 1/2)$.

As discussed in Sect. 3.1, points having $\beta > 1/2$ and $\sigma > 1/2$ are guaranteed to be passive because at each time τ they cannot be below the critical line. Points having $\beta > 1/2$ and $\sigma < 1/2$ cannot be unstable because the increase of velocity due to energy generation causes the line to become vertical, thus leading to dissipation. They however can generate instantaneous power as the slope of the line reduces; in particular if a balance is reached between energy generation and dissipation, persisting oscillations are obtained.

The existence and the characterization of these limit cycles will be discussed in the next section by means of the describing function analysis.

7. Describing Function Analysis

The passivity analysis outlined in Sect. 6 allowed us to find a worst-case condition to ensure that energy generation due to the digital nature of the virtual wall is always dominated by the intrinsic energy dissipation of the device. In particular, the condition and (6) results from the maximization (26) of the energy generated because of quantization effects.

On the other hand, the describing function [17] is a simple and powerful tool to analyze the system behavior in the "average" case, allowing us to provide estimates on the amplitude and frequency of the self-sustained oscillations (limit cycles) whose existence is predicted in Fig. 3. Moreover, since the describing function allows to analyze the stability of oscillations as well, it is possible to use it to estimate the transition on the (β, σ) plane from a stable to an unstable behavior for different system parameters.

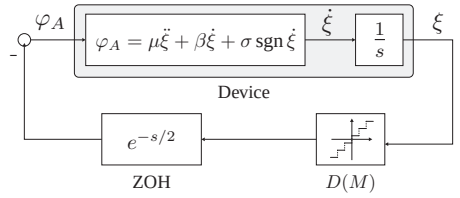

Figure 6. Block scheme for the approximate analysis.

In the following we will refer to the simplified block scheme of Fig. 6, where the dimensionless formulation (4) is used. In particular, the zero-order-hold is approximated by a time delay of $1/2$ and the encoder is represented by its describing function $D(M)$. Note that because of the integration required to obtain the position ξ from the velocity $\dot{\xi}$, the loop transfer function has a low-pass characteristic that justifies the first-order approximation involved in the application of the describing function method.

Let $G(M, \omega)$ denote the linear approximation of the nonlinear mapping (4) from φ_A to ξ representing the haptic device. From the Nyquist criterion, self-sustained oscillations are likely to arise if:

$$G(M, \omega) = -D(M)e^{-j\omega/2} \tag{36}$$

7.1. Linearization of the model of the device

If we initially suppose the existence of sinusoidal oscillation whose amplitude M is measured in encoder ticks:

$$\xi(\tau) = M\sin(\omega\tau) \qquad M>0,\ \omega>0 \tag{37}$$

then the input-output mapping between φ_A and ξ is expressed by:

$$\varphi_A(\tau) = -\mu M\omega^2\sin(\omega\tau) + \beta M\omega\cos(\omega\tau) + \\ + \sigma\,\mathrm{sgn}\left(M\omega\cos(\omega\tau)\right) \tag{38}$$

Since the Coulomb friction term maps the sinusoidal input to a square wave, the linear model:

$$\varphi_A(\tau) = M\left[-\mu\omega^2\sin(\omega\tau) + \left(\beta\omega + \frac{4\sigma}{\pi M}\right)\cos(\omega\tau)\right] \tag{39}$$

is the best linear approximation of (38) in the sense that when neglecting higher order harmonics the cross-correlation function is preserved [17]. Therefore the device is approximated by:

$$\Phi_A(M,\omega) = G(M,\omega)\,\Xi(M,\omega) = \\ = \left[-\mu\omega^2 + j\left(\beta\omega + 4\frac{\sigma}{\pi M}\right)\right]\,\Xi(M,\omega) \tag{40}$$

where $\Phi_A(M,\omega)$ and $\Xi(M,\omega)$ are the Fourier transforms of $\varphi_A(\tau)$ and $\xi(\tau)$. The dependency from the amplitude M has to be explicitly accounted because of Coulomb friction.

7.2. Describing function of the quantization

Since the quantization nonlinearity (2) is static and odd with respect to ξ, $D(M)$ is real and does not depend on the frequency ω. Under the hypothesis (37), its input-output relation (5) is approximated by the recursive expression:

$$D(M) = \frac{2}{\pi M} + \frac{4}{\pi M^2}\sum_{l=1}^{\lfloor M\rfloor}\sqrt{M^2-l^2} \tag{41}$$

According to the physical intuition we notice that quantization effects are more relevant for small motions, while the quantized measurements are good approximations of the real displacements for $M>1$. Let $D_1(M) = \frac{2}{\pi M}$, for amplitudes $M<1$, $D(M)$ can be approximated by $D_1(M)$; on the other hand, for amplitudes larger than 1, $D(M)$ quickly tends to the unity. Within the limits of the approximated quasi-linear analysis, (36) can be solved in these two separate cases, leading to two different families of oscillations.

7.3. Solution for small amplitude ($M<1$)

If we assume $D(M)\simeq D_1(M)$, the condition (36) for the existence of limit cycle is expressed by:

$$\frac{2}{\pi M}\cos\frac{\omega}{2} = \mu\omega^2\,, \qquad \frac{2}{\pi M}\sin\frac{\omega}{2} = \beta\omega + \frac{4\sigma}{\pi M} \tag{42}$$

Since the analytical computation of amplitude and frequency of the limit cycle is difficult from (42), it is more convenient to identify the (β,σ) loci characterized by a given couple (M,ω). The first admits exactly one solution for $\omega<\pi$ and states that M increases for larger values of the dimensionless inertia μ. The second equation can be hence rewritten as:

$$\sigma = \frac{1}{2}\sin\frac{\omega}{2} - \frac{\beta}{2\mu\omega}\cos\frac{\omega}{2} \qquad \omega\in[0;\pi[\tag{43}$$

Therefore, for a given frequency ω and for a given amplitude $M<1$ satisfying (42) turns out to be the equation of a line on the (β,σ) plane. Fig. 7.3 shows the contour map of lines obtained for different values of amplitude and frequency. Since σ has to be positive, it is clear that small amplitude oscillations occur only for $\sigma<1/2$ and that increments on M are translated to decrements on σ. Finally, the stability analysis of limit cycles shows that they are stable. This is the type of oscillations detected in Fig. 5.2, whose amplitude is bounded by one encoder tick.

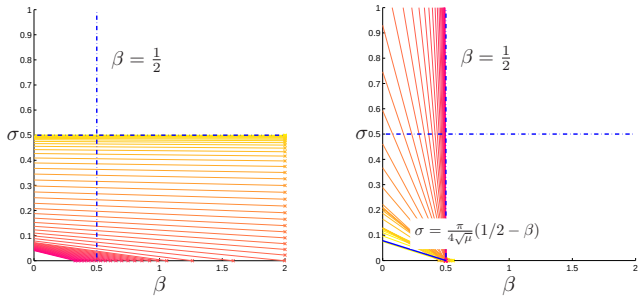

Figure 7. Contour maps of amplitude and frequency of small stable ($M<1$, left) and large unstable oscillations ($M>1$, right) for $\mu=5$.

7.4. Solution for large amplitude ($M>1$)

On the other hand, for large amplitudes the encoder describing function is approximately $D(M)\simeq 1$ and (36) reduces to the Nyquist criterion; therefore the oscillations found in this case represent the transition from stability to instability. In particular, we have:

$$\cos\frac{\omega}{2} = \mu\omega^2\,, \qquad \sin\frac{\omega}{2} = \beta\omega + \frac{4\sigma}{\pi M} \tag{44}$$

As in the previous case, the first equation admits solution only for $\omega<\pi$, while the second leads to:

$$\sigma = \frac{\pi M}{4}\left(\sin\frac{\omega}{2} - \beta\omega\right) \qquad \omega\in[0;\pi[\tag{45}$$

The term in parentheses is positive only if $\beta\le 1/2$ and, as Fig. 7.3 shows, large amplitude oscillations are only possible in regions having small viscous friction. Moreover,

if the frequency is sufficiently small that $\cos(\omega/2)$ and $\sin(\omega/2)$ can be approximated by their series expansions. Since $|\dot{\xi}_0| = M\omega$ (i.e. the maximum velocity for the pseudo-sinusoidal oscillations is $M\omega$) and in the (β, σ) plane the linearization of (45) represents a line whose slope is $-|\dot{\xi}_0|$ and, analogously to the result of the passivity analysis, it is a stability bound. Finally, noting that $\omega \geq 1/\sqrt{\mu}$, the system is conditionally stable only if:

$$\sigma \geq \frac{\pi}{4\sqrt{\mu}} \left(\frac{1}{2} - \beta \right) \tag{46}$$

Below this line the Nyquist criterion allows to conclude, in the limits of this approximate analysis, that the system (4) is unstable. Note the line depends on the dimensionless inertia μ (see Tab. 1). Also, with respect to the passivity analysis, this new critical line rotates about the point $(\frac{1}{2}, 0)$ instead of $(\frac{1}{2}, \frac{1}{2})$. This difference is consistent with the fact that (6) is obtained through the worst-case analysis outlined in Sect. 6, while (46) describes the "average" behavior with respect to the quantization and Coulomb nonlinearities.

8. Conclusions

This work has examined the stability of a haptic display. It relates the inertia, viscous, and Coulomb friction of the device to the controller stiffness, sampling rate and encoder resolution. Using a dimensionless approach to simplify the developments and highlight critical parameter combinations, a general stability criterion is presented.

Examining the instantaneous power balance of mechanical dissipation and artificial generation, distinct behaviors are identified and related to the system parameters. The behaviors are categorized as passive, locally stable, limit cycles, and unstable. In comparison to this worst case analysis, a describing function investigation provides insights on the average system behavior. The results obtained the two different approaches are consistent and show that quantization causes stable limit cycles in systems with little Coulomb friction, while conditional stability occurs for limited viscous damping. Finally, note that both the computational delay and the limitations on the current amplifier's bandwidth, although not explicitly considered in this paper, can be easily accounted in the describing function setting.

We hope these insights will lead to better controllers for existing haptic devices and ultimately improve the design of future haptic displays.

Acknowledgments

The authors wish to thank François Conti, Katherine Kuchenbecker and Neal Tanner for their help in providing the parameters of haptic devices reported in Table 2.

References

[1] T. Massie and J. Salisbury, "The phantom haptic interface: a device for probing virtual objects," in *ASME Winter Annual Meeting*, vol. 55-1, New Orleans, LA, 1994, pp. 295–300.

[2] F. Barbagli and J. Salisbury, "The effect of sensor/actuator asymmetries in haptic interfaces," in *IEEE Haptics Symposium*, Los Angeles, CA, March 2003, pp. 140–147.

[3] J. Colgate, P. Grafing, M. Stanley, and G. Schenkel, "Implementation of stiff virtual walls in force-reflecting interfaces," in *IEEE Virtual Reality Symposium*, 1993, pp. 202–208.

[4] J. Colgate and G. Schenkel, "Passivity of a class of sampled-data systems: Application to haptic interfaces," in *American Control Conference*, Baltimore, Maryland, June 1994, pp. 3236–3240.

[5] B. Gillespie and M. Cutkosky, "Stable user-specific rendering of the virtual wall," in *ASME IMECE*, vol. DSC-Vol. 58, Atlanta, GA, November 1996, pp. 397–406.

[6] N. Hogan, "Controlling impedance at the man/machine interface," in *Proceedings IEEE International Conference on Robotics and Automation*, 1989, pp. 1626–1631.

[7] B. Hannaford and J. Ryu, "Time domain passivity control of haptic interfaces," in *Proceedings of the IEEE International Conference on Robotics and Automation*, Seoul, Korea, May 2001, pp. 1863–1869.

[8] B. Miller, J. Colgate, and R. Freeman, "On the role of dissipation in haptic systems," *IEEE Transactions on Robotics*, vol. 20, no. 4, pp. 768–771, August 2004.

[9] M. Mahvash and V. Hayward, "High fidelity passive force reflecting virtual environments," *IEEE Transactions on Robotics*, 2004, in press.

[10] J. J. Abbott and A. M. Okamura, "A sufficient condition for passive virtual walls with quantization effects," in *ASME IMECE International Symposium on Advances in Robot Dynamics and Control*, 2004, in press.

[11] N. Diolaiti, G. Niemeyer, F. Barbagli, and J. Salisbury, "A passivity criterion for haptic devices," in *IEEE International Conference on Robotics and Automation*, 2005, submitted.

[12] K. Kuchenbecker, J. Park, and G. Niemeyer, "Characterizing the human wrist for improved haptic interaction," in *ASME IMECE International Mechanical Engineering Congress and Exposition*, Washington, D.C. USA, November 16-21 2003.

[13] K. Kuchenbecker and G. Niemeyer, "Canceling induced master motion in force-reflecting teleoperation," in *ASME IMECE Symposium on Advances in Robot Dynamics and Control*, Anaheim, CA, November 13 - 19 2004.

[14] C. Zilles, "Haptic rendering with the toolhandle haptic interface," Master's thesis, Massachusetts Institute of Technology, Cambridge, MA, 1995.

[15] A. van der Schaft, *L_2-Gain and Passivity Techniques in Nonlinear Control*, ser. Communication and Control Engineering. Springer Verlag, 2000.

[16] J. Willems, "Dissipative dynamical systems, part i: General theory," *Arch. Rat. Mech. An.*, vol. 45, 1972.

[17] J. Slotine and W. Li, *Applied Nonlinear Control*. Englewood Cliffs, NJ: Prentice Hall, 1991.